



**HAL**  
open science

# Increased exposure of coastal cities to sea-level rise due to internal climate variability

Melanie Becker, M. Karpytchev, A. Hu

## ► To cite this version:

Melanie Becker, M. Karpytchev, A. Hu. Increased exposure of coastal cities to sea-level rise due to internal climate variability. *Nature Climate Change*, 2023, 13 (367–374), 10.1038/s41558-023-01603-w . hal-04012725

**HAL Id: hal-04012725**

**<https://cnrs.hal.science/hal-04012725>**

Submitted on 8 Jan 2024

**HAL** is a multi-disciplinary open access archive for the deposit and dissemination of scientific research documents, whether they are published or not. The documents may come from teaching and research institutions in France or abroad, or from public or private research centers.

L'archive ouverte pluridisciplinaire **HAL**, est destinée au dépôt et à la diffusion de documents scientifiques de niveau recherche, publiés ou non, émanant des établissements d'enseignement et de recherche français ou étrangers, des laboratoires publics ou privés.

# Increased exposure of coastal cities to sea-level rise due to internal climate variability

M. Becker<sup>1</sup>, M. Karpytchev<sup>1</sup> & A. Hu<sup>2</sup>

1. LIENSs UMRi 7266 CNRS, University of La Rochelle, France

2. National Center for Atmospheric Research, Colorado, USA

Accepted Manuscript for Nature Climate Change (2023)

Becker, M., Karpytchev, M. & Hu, A. Increased exposure of coastal cities to sea-level rise due to internal climate variability. *Nat. Clim. Chang.* **13**, 367–374 (2023). <https://doi.org/10.1038/s41558-023-01603-w>

Corresponding author: Mélanie Becker ([mbecker@univ-lr.fr](mailto:mbecker@univ-lr.fr))

## Abstract

Adaptation to future sea-level rise is based on projections of continuously improving climate models. These projections are accompanied by inherent uncertainties, including those due to internal climate variability (ICV). The ICV arises from complex and unpredictable interactions within and between climate-system components, rendering its impact irreducible. Although neglecting this uncertainty can lead to an underestimation of future sea-level rise, its estimation and impacts have not been fully explored. Combining the Community Earth System Model version 1 Large Ensemble experiments with power-law statistics, we show that, by 2100, if the ICV uncertainty reaches its upper limit, new sea-level-rise hotspots would appear in Southeast Asian megacities (Chennai, Kolkata, Yangon, Bangkok, Ho Chi Minh City and Manila), in western tropical Pacific Islands and the Western Indian Ocean. The better the ICV uncertainty is taken into account and correctly estimated, the more effective adaptation strategies can be elaborated with confidence and actions to follow.

*Keywords: Sea level · Internal climate variability · GCM · Power-law statistics · CESM1-LE*

---

Distinguishing the human activity signature in past and ongoing sea-level changes is a challenging topic of intense studies<sup>1–6</sup>. A major obstacle for reliable detection of the anthropogenic signals originates from substantial contribution of natural fluctuations to the sea-level changes. These fluctuations mirror the complex climate-system dynamics, commonly called internal climate variability (ICV). The ICV is

4 generated by chaotic interactions within and between the atmosphere, hydrosphere, cryosphere, biosphere  
5 and the solid-Earth processes occurring over an extremely wide range of time and space scales<sup>7,8</sup>. These  
6 interactions can manifest as cycles, instabilities or irregular oscillations of the climate system<sup>9,10</sup>. One  
7 example of well-known manifestation of the internal variability in the climate system is the El Niño/  
8 Southern Oscillation<sup>8</sup>. The practical importance of the ICV is rooted in its chaotic nature, leading to an  
9 irreducible uncertainty in the sea-level projections<sup>1,11–17</sup>.

1 A commonly used approach for estimating the ICV uncertainty in future sea-level changes is based on  
2 large ensembles (LEs) of global climate models (GCMs)<sup>12,13,18,19</sup>. An LE is a set of numerical simulations  
3 conducted with the same GCM and forcing scenario but with slightly different initial conditions<sup>20</sup>. The  
4 spread among the ensemble members mimics the chaotic and unpredictable nature of climate and  
5 characterizes the ICV intensity, while the changes due to external forcing are usually represented by the  
6 average of the LE realizations<sup>8,21</sup>. By using a 40-member Community Climate System Model version 3 LE,  
7 Hu and Deser<sup>13</sup> have reported that the ICV contribution to the mean sea-level changes between 2041–2060  
8 and 1980–1999 varies regionally by a factor of two among the LE members, while the global mean sea-level  
9 rise (SLR) remains almost unaffected by the ICV. Substantial impact of the ICV on the regional mean sea  
0 level was also confirmed by analysis of the multimodel ensemble spread (for example, Coupled Model  
1 Intercomparison Project Phases 5/6 (CMIP5/6)<sup>14,17,22–24</sup>). However, the multimodel ensemble spread arises  
2 from both ICV and specific parameterizations in the modelling process<sup>14,17,22,23,25,26</sup>. Thus, the uncertainty  
3 estimated from the multimodel ensemble is rather a measure of consensus within the multimodel ensemble,  
4 which is important but distinct from evaluations of the ICV uncertainty in LEs<sup>10,14,27–29</sup>.

6 There exists also an alternative for evaluating the ICV contribution that is based on the specific temporal  
7 behaviour of sea-level fluctuations. It has been widely recognized that the sea-level fluctuations are  
8 organized over an extremely broad range of periods, in such way that their power spectral density,  $S$ , closely  
9 follows a power-law spectrum ( $f$ , frequency) defined by an exponent  $\beta$  (ref. <sup>30</sup>):

$$S \sim f^{-\beta} \quad (1)$$

1 The power-law character of sea-level fluctuations described by equation (1) is a manifestation of the  
2 complex ICV structure<sup>31</sup>. Analysis of the 100-yr-long sea-level records shows that the scaling exponent  $\beta$  is  
3 site dependent and varies:  $0 < \beta < 2$ <sup>1,32–37</sup>. The scaling with  $\beta > 0$  corresponds to persistent sea-level  
4 fluctuations with long-term correlations (long-term memory), while  $\beta = 0$  indicates a signal indistinguishable  
5 from a random process with no memory (white noise). A particular feature of the long-term memory

6 processes ( $\beta > 0$ ) is that they can generate long-term trend-like spontaneous deviations that can considerably  
7 mask the trend induced by external forcing. Concerning the GCMs, it is a long-standing question whether  
8 they can reproduce the power-law behaviour detected in observed sea-level records<sup>1,32–36</sup>. Extensive  
9 comparison of 36 CMIP5 GCMs with observations<sup>38</sup> showed that a majority of GCMs overestimate the  
0 power-law character of observed sea-level variations. The best performance was obtained by Community  
1 Earth System Model version 1 (CESM1), which reproduced the observed sea-level scaling in three-quarters  
2 of the sea-level records analysed.

3  
4 A logical follow-up is to assess the CESM1-LE ability to reproduce the ICV uncertainty in sea-level  
5 projections and to constrain uncertainties in the future mean sea-level changes. These should not be confused  
6 with the changes in the mean sea level driven by the external forcing. However, in long-term correlated  
7 records, the ICV contribution may look like a trend indistinguishable from an externally generated trend. By  
8 consequence, the coastal population can suffer from the ‘apparent’ sea-level trend-like changes generated  
9 by the ICV in a similar way as from the externally driven changes because it is the rate of SLR that matters  
0 for coastal defences and not only the origin of sea-level drivers. This point is essential for developing  
1 effective strategies and design responses for coastal communities facing SLR in a warming world. To guide  
2 our investigations, we (1) explore the regional variations in the power-law exponent of sea-level fluctuations;  
3 (2) compare the ICV uncertainty estimated from CESM1-LE spread with that derived from the power-law  
4 statistics; (3) evaluate, in selected global coastal cities, the maximum expected ICV contribution to sea-level  
5 changes by 2100 and (4) discuss the ICV uncertainty impact on coastal flooding.

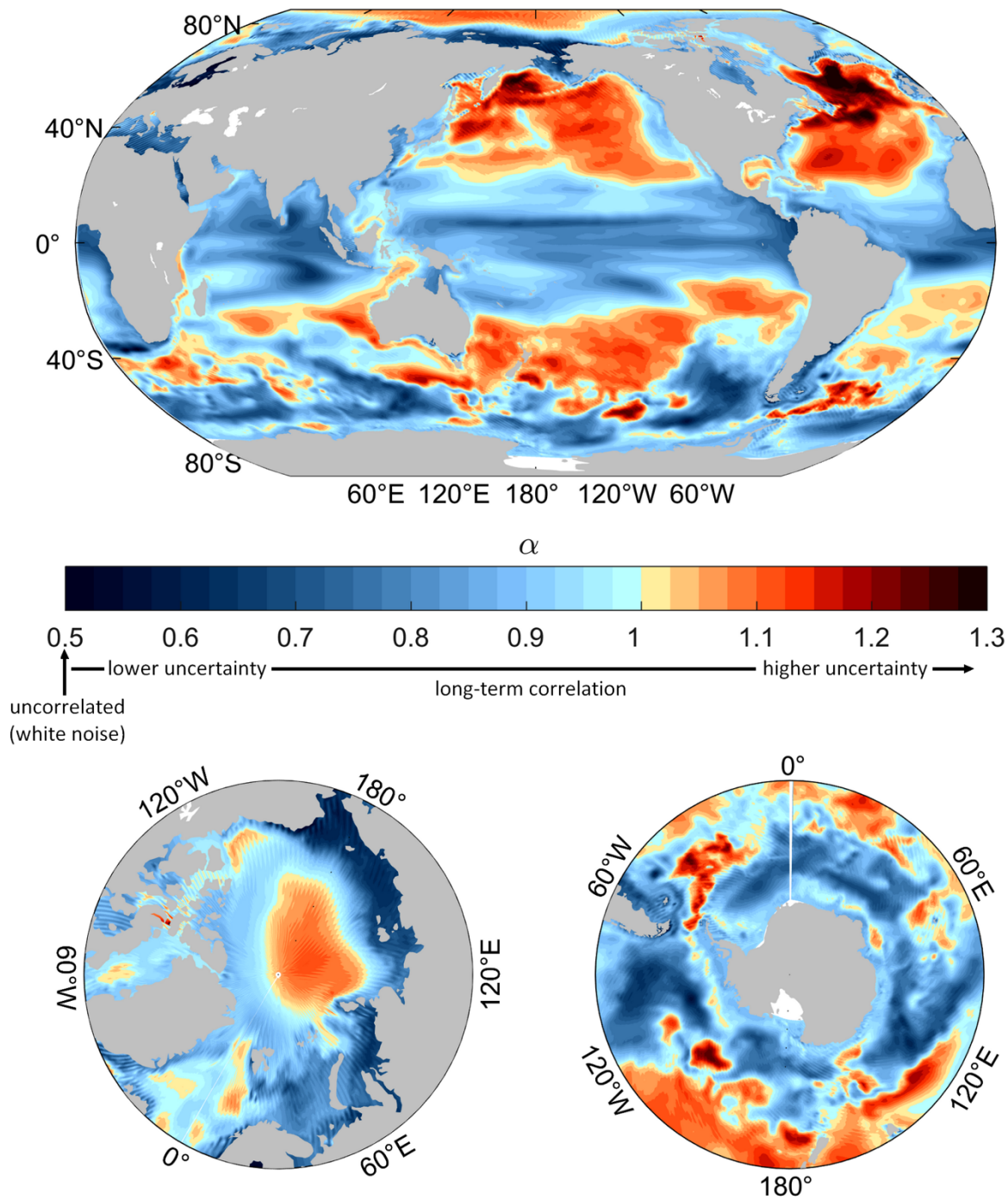
### 6 **Scaling behaviour of sea-level fluctuations**

7 The scaling properties of sea-level fluctuations can be measured by using the well-established detrended  
8 fluctuation analysis (DFA)<sup>39</sup>. Compared with other standard tools (for example, Fourier spectrum or Hurst  
9 rescaled-range analysis<sup>40</sup>), the DFA $n$  effectively eliminates polynomial trends of order  $n - 1$  in the original  
0 data and permits reliable detection of long-term correlations in nonstationary time series<sup>39</sup>. The DFA  
1 analyses scaling properties of the fluctuation function,  $F(s)$ , which characterizes sea-level fluctuations in the  
2 non-overlapping time windows of size  $s$ <sup>39,41</sup>. The DFA provides a single parameter—the scaling exponent  $\alpha$   
3 (also called Hurst exponent)—to quantify the correlation properties of the time series (see Methods for more  
4 details). A power-law relation between  $F(s)$  and the segment’s size  $s$  indicates the presence of long-term  
5 correlations:  
6

$$7 \quad F(s) \sim s^\alpha \quad (2)$$

8 This exponent is related to the power spectral density exponent  $\beta$  in equation (1) by  $\beta = 2\alpha - 1$  (ref. <sup>41</sup>).  
9 Different types of temporal behaviour can be identified as uncorrelated signals for  $\alpha = 0.5$  (white noise) and  
0 long-term correlations for  $\alpha > 0.5$ . We apply scaling analysis to sea-level fluctuations simulated by the  
1 1,800-yr-long CESM1 pre-industrial control run<sup>21</sup> (see Methods for CESM1 details; Extended Data Fig. 1),  
2 with the exponent  $\alpha$  estimated by DFA3 (ref. <sup>42</sup>). In the following, we use the term ‘sterodynamic sea level’  
3 for designating a sum of sea-level changes due to thermosteric effect and dynamical ocean adjustment  
4 computed by CESM1 (ref. <sup>43</sup>). It does not include yet-unmodelled changes in sea level due to land-based ice  
5 or to land movement. The spatial variations of the scaling exponent appear to be not randomly dispersed but  
6 remarkably organized in large-scale patterns, highlighting regional similarities in sea-level temporal  
7 behaviour within large areas (Fig. 1). One can say that, globally, the oceans are characterized by scaling  
8 exponents ranging between 0.5 and 1.0, with the lowest values of 0.5 to 0.6 in the Arctic Ocean region,  
9 specifically in the Bering Sea and in the East Siberian Sea. As a larger scaling exponent means a more  
intense energy transfer across the spectrum of sea-level fluctuations (equation (1)), it seems reasonable to  
suggest that its enhanced values ( $\alpha > 1$ ) are associated with the mostly energetic extratropic regions hosting  
strong ocean currents such as subpolar gyre regions, the Kuroshio extension in the North Pacific, the North  
Atlantic Drift current and the Antarctic Circumpolar Current in the southern oceans. The scaling exponent  
patterns in Fig. 1 are in accordance with the results of previous studies that have investigated the GCM  
spatial structure of the sea-level variability<sup>44</sup>. For example, Monselesan et al.<sup>44</sup> noticed in the 500 yr pre-  
industrial runs of CMIP5 models that, on longer time scales ( $>5$  yr), maximum sea-level variance moves to  
the extratropics. It is worth noting that with increasing scaling exponent  $\alpha$  (that is, with increasing strength  
of the long-term correlations), the range of the ICV uncertainty increases and, thus, so does the uncertainty  
about the sea-level change.

# Scaling exponent $\alpha$ of sterodynamic sea level



0  
1  
2  
3  
4  
5

**Fig. 1 | Scaling exponent  $\alpha$  of sterodynamic sea-level fluctuations.** Estimated from the 1,800 yr CESM1 pre-industrial control run by DFA3 with windows of size  $s$  ranging from 1 to 95 yr. For uncorrelated data,  $\alpha = 0.5$  (white noise), and for long-term correlated data,  $\alpha > 0.5$ .

## ICV uncertainty contribution to sea level changes

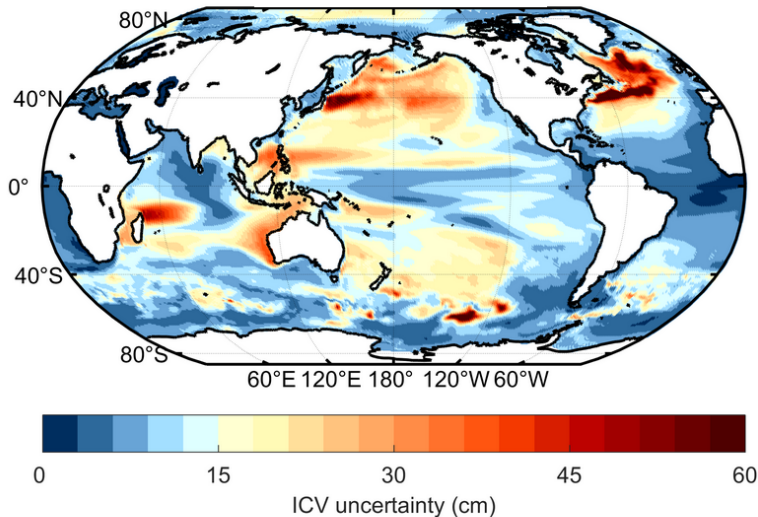
The estimates of change in climate variables are often based on differences between their averages computed over several decades<sup>12,13,45</sup>. Here, we estimate the ICV contribution to expected changes in the mean sea level between 1920 and 2005. A relevant quantity for that,  $\Delta$ , is a product of the sea-level regression line slope (cm yr<sup>-1</sup>) and the duration. It represents a change of the mean sea level over the considered period<sup>46</sup> (see Methods for details).  $\Delta$  is widely used in sea-level studies; for example, the global mean sea-level trend during the twentieth century is  $\sim 0.17$  cm yr<sup>-1</sup> (ref. <sup>47</sup>), which corresponds to a 17 cm increase between the beginning and the end of the twentieth century. For each of the 40 members in the CESM1-LE historical simulations, the modelled sea-level change,  $\Delta_{i=1\dots 40}$ , is estimated as explained in the preceding. We measure the spread between the  $\Delta_{i=1\dots 40}$ , by two standard deviations ( $2\sigma$ , called hereafter  $ICV_{CESM1-LE}$ ; Extended Data Fig. 2), giving a direct measure of the ICV contribution to the changes in the mean sea level expected by 2005 relative to 1920. Furthermore, we employ the statistics of power-law correlated series to determine the range of spontaneous trend-like sea-level fluctuations in the CESM1 historical run caused by the ICV. To do this, we use the scaling exponent  $\alpha$  previously estimated and, for every  $\alpha$ , calculate the confidence interval within which the spontaneous trend-like fluctuations occur with the 95% probability<sup>46,48,49</sup> by 2005 relative to 1920 (called hereafter  $ICV_{power-law}$ ; see Methods for more details; Extended Data Fig. 3). This approach generalizes the analysis of sea-level variance by Monselesan et al.<sup>44</sup> in the sense that it accounts for the long-term sea-level correlations by modulating the sea-level variance by a factor depending on the scaling exponent  $\alpha$ <sup>46,48,49</sup>. Moreover, the power-law statistics provide the bounds on the uncertainties of the steric sea-level changes simulated by CESM1 on annual to multi-decadal timescales. This is an important advance compared with common techniques such as, low-pass filtering based on smoothing sea-level fluctuations used in IPCC Fifth Assessment Report and Sixth Assessment Report, which suppresses sea-level variations on timescales longer than a few decades and consequently underestimate the long-term part of the ICV contribution<sup>47,50</sup>.

The comparison of  $ICV_{power-law}$  with  $ICV_{CESM1-LE}$  (Fig. 2) reveals close relations between the approaches in general and even a linear correlation between these two metrics in many oceanic regions. Moreover, a larger dispersion between CESM1-LE members at a given location corresponds systematically to a larger spread of naturally occurring sea-level trends predicted by the statistics of deviations in the power-law correlated time series. A closer similarity between spatial patterns of ICV uncertainty in both methods seems to be associated with the regions of energetic oceanic currents. Note, however, that no universal linear relationship is obvious in some regions, as in the Pacific inter-tropical or the North Indian Ocean. Notice that in the North Atlantic and South Indian Ocean, although the ICV uncertainty patterns are coherent between both metrics, the ICV estimated from the power-law statistics is nearly four to five times greater

9 than variability of the ensemble estimates. Thus, the power-law statistics seems to predict a larger ICV  
0 contribution in the mean sea-level changes than that derived from the CESM1-LE spread. This probably  
1 points to a yet small sampling size of the LE or to existence of a part of the ICV uncertainty that is not  
2 captured by the specific method of perturbing initial conditions in CESM1-LE. It can also be due to  
3 limitation of the universal scaling hypothesis in equation (1).

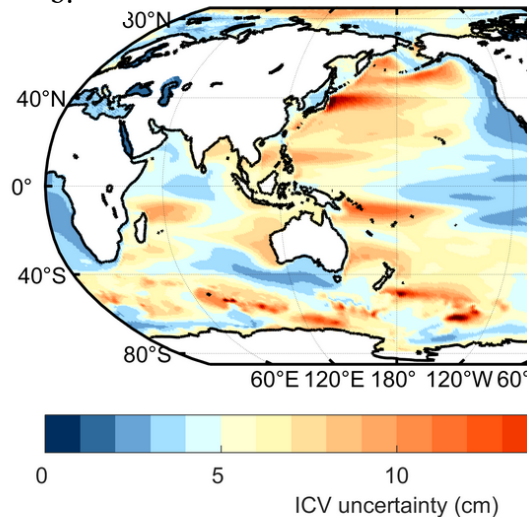
a.

Power-law statistics



b.

CESM1-LE spread



c.

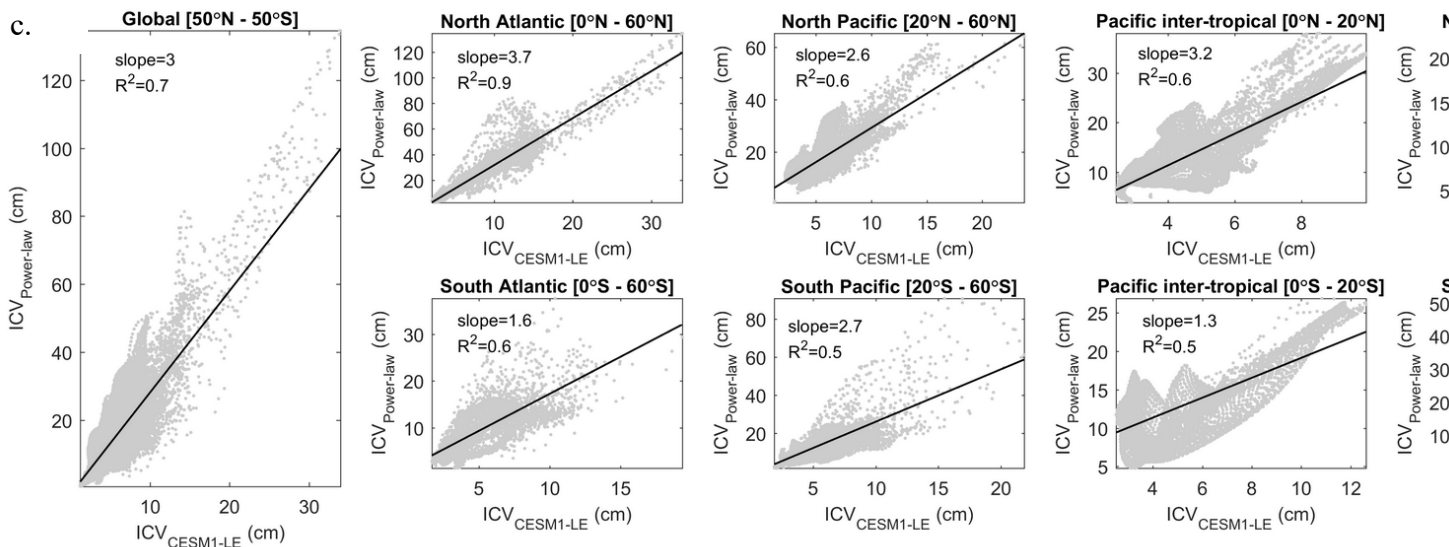
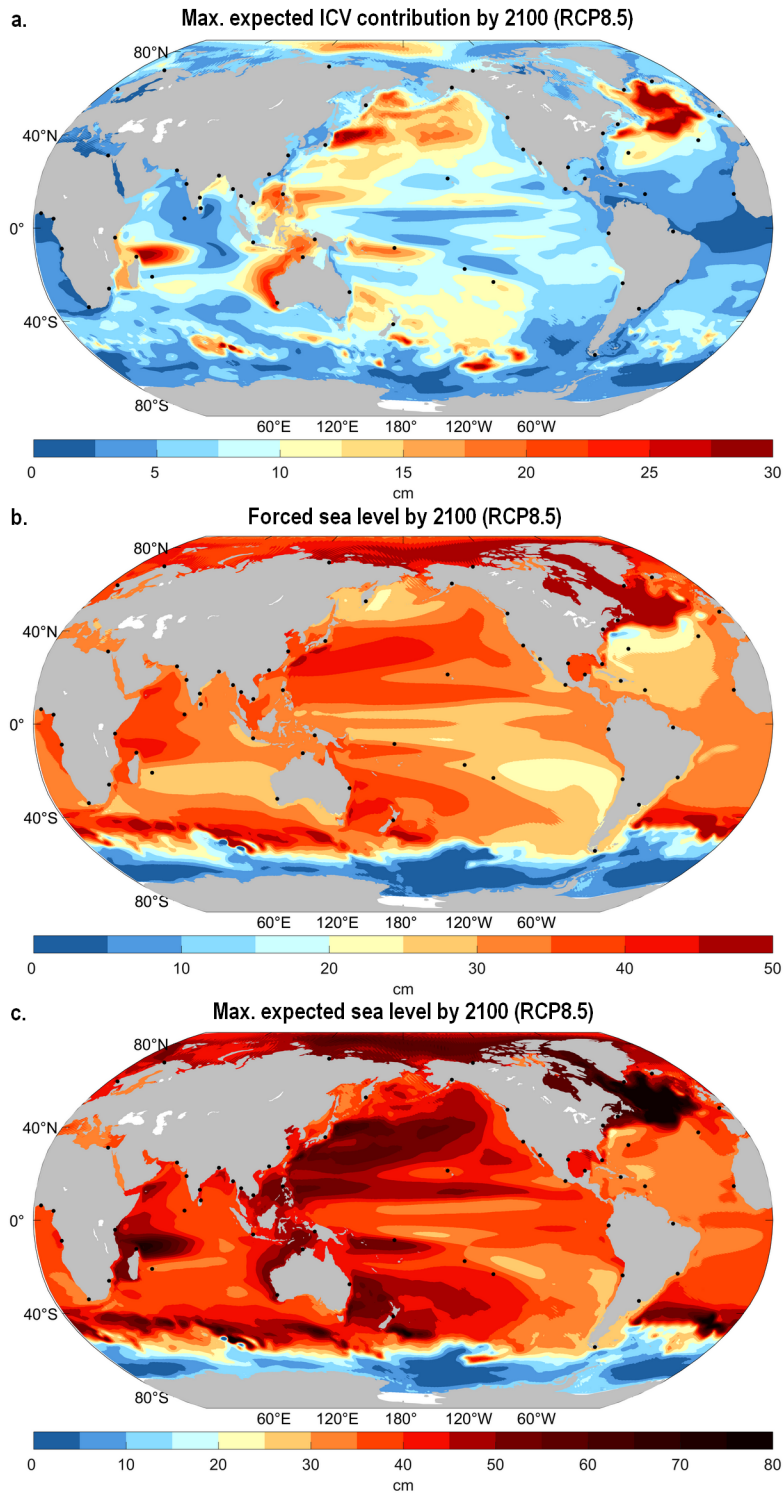


**Fig. 2 | Geographical distribution of the ICV uncertainty range of steredynamic sea-level changes by 2005 (relative to 1920) predicted by the power-law statistics (two-sided 95% confidence interval) (a) and 40-member CESM1-LE historical simulation spread ( $2\sigma$ ) (b). The uncertainty in the mean sea-level changes by 2005 (relative to 1920) predicted by the power-law statistics ( $ICV_{power-law}$ ) and the 40-member CESM1-LE historical simulation spread ( $ICV_{CESM1-LE}$ ). The slope ( $P < 0.001$ ) and  $R^2$  of the linear regression are given for comparison at the global and regional scale.**

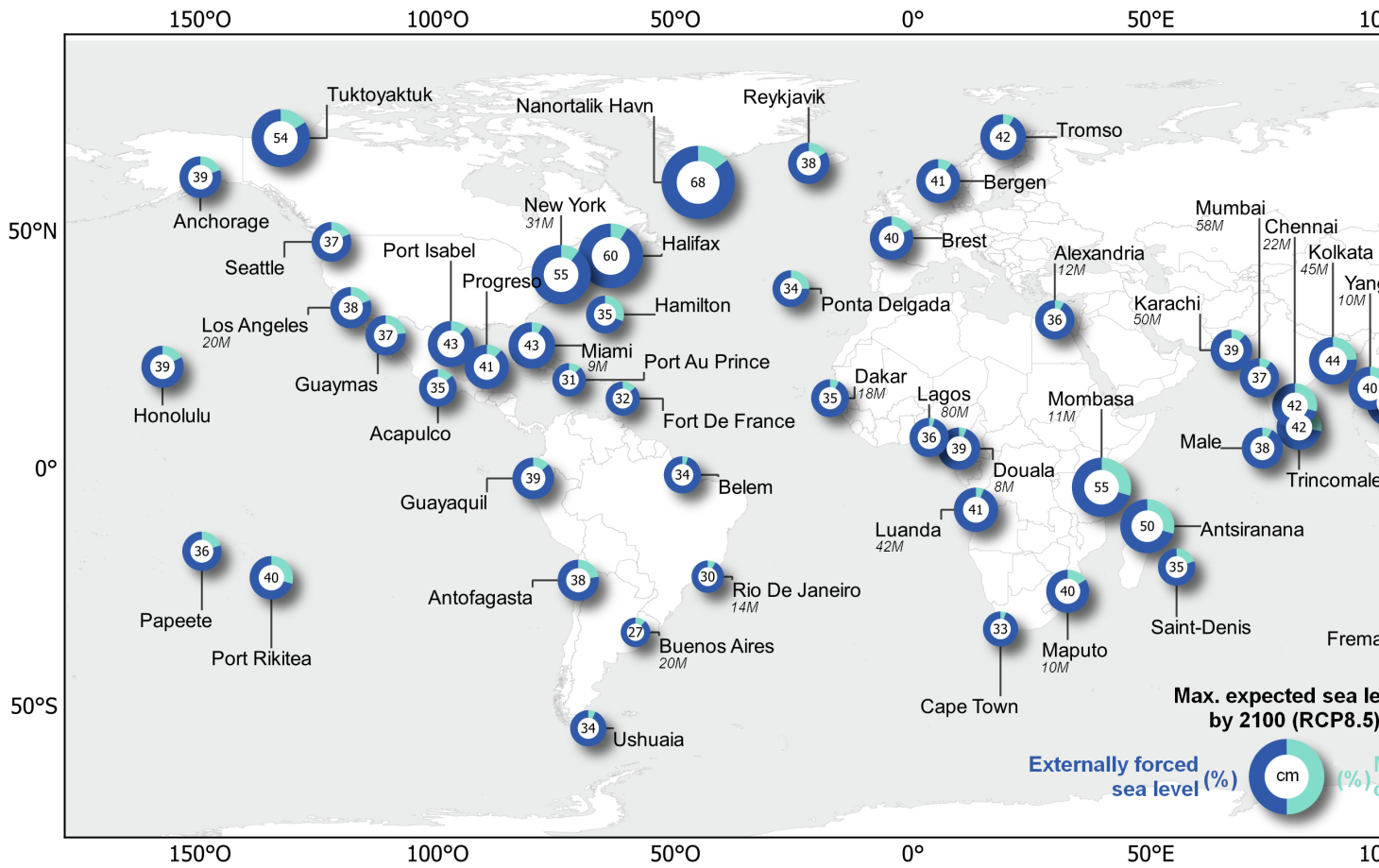
## ICV uncertainty and future sea-level hotspots

We now investigate the ICV contribution to the projected mean sea-level change by 2100 under a carbon high-emissions global warming scenario (representative concentration pathway (RCP) 8.5). The  $ICV_{power-law}$  exceeds the  $ICV_{CESM1-LE}$  by a factor of two globally and, particularly, by a factor of six along the coasts of East Africa, west Australia, Southeast Asia and west United States (Extended Data Fig. 4). In the perspective of evaluating future coastal flood risks, we focus on upper boundaries of the projected sea-level range<sup>51</sup> and consider the maximum expected ICV contribution obtained from the power-law statistics (an upper bound of the two-sided 95% confidence interval). The maximum expected ICV contribution ranges, typically, from 2–17 cm, but there are distinct regions where the value exceeds 25 cm, as in the North Atlantic, the North Pacific and along the Australian west coast (Fig. 3a). We defined the maximum expected SLR (Fig. 3c) as the sum of expected forced sea level (Fig. 3b), obtained from the ensemble mean of SLR from CESM1-LE, and of the maximum expected ICV contribution obtained from the power-law statistics (an upper bound of the two-sided 95% confidence interval; Fig. 3a). Defined in this way, the maximum expected SLR is then an upper-bound scenario, giving important information for coastal planning purposes. For example (Fig. 4), the maximum sea level at New York by 2100 (relative to 2006) is expected to increase by 55 cm, in part due to the ICV being ~6 cm (11%) as evaluated from the power-law statistics. Future steric sea level is more predictable in some regions than in others (Fig. 4). We show that half of the considered cities could be seriously threatened by a sea-level increase of over 20%, and up to 50%, due solely to local amplification of the ICV contribution (Fig. 4 and Extended Data Fig. 5). This could happen, for example, in Tuvalu (Funafuti), French Polynesia (Rikitea) and along the southwestern coast of New Guinea (Amamapare), where the expected sea level could increase by ~14 cm due to ICV, versus ~31 cm induced by expected forced sea level, reaching a height of ~45 cm by 2100 (relative to 2006). In the Indian Ocean, several megacities, as Mombasa (Kenya), Chennai (India), Kolkata (India) and Ho Chi Minh City (Vietnam) in the South China Sea, will probably follow a similar route in facing an important expected sea-level increase of ~37%, due solely to the ICV contribution. Note that the magnitude of the expected sea-level change is largely uncertain at Fremantle and Darwin, along the western coast of Australia and the megacity of Manila (Philippines), where the ICV could amplify the externally forced sea level by 91%, 53% and 58%, respectively (Fig. 4 and Extended Data Fig. 5). If the ICV upper limit is reached, new SLR hotspots will peak in Southeast Asian megacities with the ICV part in the maximum expected SLR of, at least, ~20% at Chennai, Kolkata, Yangon, Bangkok, Ho Chi Minh City and Manila, and up to ~30% in the western tropical Pacific Islands and in the Western Indian Ocean. Obviously, such substantial ICV fluctuation would place millions of people at significantly larger risk by 2100 than that predicted without considering the ICV.



202  
203  
204  
205  
206  
207  
208

**Fig. 3 | Sterodynamic SLR by 2100 under RCP 8.5 (relative to 2006).** a. Maximum expected ICV contribution (= 95% confidence interval upper bound) obtained from the power-law statistics; b. Externally forced sea level rise from CESM1-LE and c. Maximum expected sea level rise, defined as the sum of externally forced sea level and of the maximum expected ICV contribution obtained from the power-law statistics. The black dots are the locations of the major ports world-wide (obtained from the World Port index database, <https://msi.nga.mil/Publications/WPI> ).



209  
210

211 **Fig. 4 | Upper-bound scenario of the expected stereodynamic SLR by 2100 under RCP 8.5 (relative to 2006).** The size  
 212 attached to them represent the maximum expected SLR, defined as the sum of externally forced sea level obtained from the  
 213 CESM1LE (blue) and the maximum expected ICV contribution obtained from power-law statistics (turquoise) corresponding  
 214 interval upper bound. Probability of a larger ICV contribution than that shown by the turquoise part of circles is 2.5%. This  
 215 worldwide. Population previsions for the megacities by 2100 are given in millions under the Shared Socioeconomic Pathway  
 216 Basemap from Natural Earth (<https://www.naturalearthdata.com>).

## ICV can increase frequency of future extreme sea levels

Small increases in mean sea level can make extreme sea-level events much more frequent<sup>52,53</sup>. Assuming the Gumbel distribution to be adequate for characterizing sea-level extremes, the frequency  $N$  of exceeding a given level  $h$  is given by<sup>53</sup>:

$$N = \exp(h/\lambda) \quad (3)$$

with  $\lambda$  a site-dependent scale parameter. As a first estimate, we assume that the Gumbel law scale parameter remains unchanged in the future. At sea-level stations, where the values of  $\lambda$  are available<sup>54</sup>, we compute, using equation (3), the changes in frequencies of extreme sea-level events induced by the SLR with and without accounting for the ICV contribution (Table 1). By 2100 and under RCP 8.5, at New York, the rare events are expected to occur 18 times more frequently than in 2006 and even 25 times more often if the upper limit of ICV uncertainty is reached. There are, however, some regions where this issue becomes much more critical by 2100. For example, in Manila, with no ICV contribution considered, the rare events are expected to occur also 18 times more frequently by 2100, as in New York. However, the ICV contribution can drastically change the future of Manila by increasing the extreme-events frequency by a factor of 96 if the upper limit of ICV uncertainty is considered (Table 1). An even more striking ICV contribution can be expected at Darwin, Mombasa, Funafuti, Fremantle and Ho Chi Minh City (Table 1), where the impact of externally forced SLR can be amplified by the ICV by a factor of seven to nine. For example, the Funafuti atoll is expected to face, due to externally driven SLR, a 1-in10,000 yr event to appear every  $10,000/175 \approx 57$  yr (Table 1). However, the ICV can decrease this return period to  $\sim 6$  yr, making 1-in-10,000 yr events (perhaps never yet observed by the Funafuti population) very likely to occur, on average, every 6 yr by about 2100.

Sea-level allowance is another useful quantity of interest for the design of coastal defence, quantifying the increase of defence structures needed to maintain its current flood probability under future SLR<sup>53,55–57</sup>.

The sea-level allowance ( $A$ ) can be calculated as<sup>55</sup>:

$$A = h + \frac{\sigma^2}{(2\lambda)} \quad (4)$$

where  $h$  is the externally forced SLR by 2100 derived from CESM1-LE, the uncertainty  $\sigma$  is the maximum expected ICV contribution by 2100 from power-law statistics and  $\lambda$  is the Gumbel scale parameter from (ref. <sup>54</sup>) (as in Equation 3 and Table 1). Note that  $A$ , as a first approximation, excludes effects of wave set-up and run-up, which may be important in some regions<sup>58</sup>. We focus on the second term in Equation 4, which

reflects the additional impact of the ICV contribution on the defence structure increase needed by 2100 under RCP 8.5.

The ICV contribution can reach about one-third of that due to the externally forced SLR at Rikitea, Wellington and Ho Chi Minh City (Table 1). It can reach half of the externally forced SLR at Darwin, Mombasa, Manila and Funafuti and be comparable to the externally forced SLR at Fremantle (Table 1). Therefore, there is enhanced probability of a real danger for all these regions, where the ICV fluctuations are large enough to increase the externally forced sea level, topping up the frequency of extreme sea-level events and amplifying the flooding hazard and the human impacts.

**Table 1 | Maximum expected ICV contribution impact, by 2100 and under RCP 8.5 (relative to 2006), on the extreme sea-level event frequencies and the increase of the defence structures needed to maintain the current flood probability under future sea level**

City	Location (latitude, longitude)	$h$ (cm)	$\sigma$ (cm)	$\lambda$ (cm)	$N_h = \exp(h/\lambda)$	$N_{h+\sigma} = \exp((h + \sigma)/\lambda)$	Increase (cm) of the defence structures needed by 2100 due to maximum expected ICV contribution ( $\sigma^2/(2\lambda)$ )	Increase of the defence structures needed by 2100 due to maximum expected ICV contribution compared with $h$ (%)
New York	40.70° N, 74.02° W	49	6	17	18	25	1	2
Manila	14.58° N, 120.97° E	33	19	11.4	18	96	16	48
Rikitea	23.12° S, 134.97° W	28	12	7.5	44	215	9	33
Yangon	16.77° N, 96.17° E	32	8	6.5	148	471	4	13
Darwin	12.47° S, 130.85° E	33	17	8.3	52	427	18	56
Mombasa	4.07° S, 39.67° E	39	16	7.7	151	1,251	17	45
Funafuti	8.52° S, 179.19° E	31	13	6	175	1,530	14	45
Fremantle	32.05° S, 115.75° E	27	25	12.6	9	61	24	89
Wellington	41.28° S, 174.78° E	39	11	6.5	403	2,191	9	24
Ho Chi Minh City	10.77° N, 106.72° E	35	12	5.9*	377	2,882	12	35

\*From Vung Tau tide-gauge record located ~60 km from Ho Chi Minh City.

## Conclusion

The sea-level projections are accompanied by inherent uncertainties of which a substantial part arises from complex and unpredictable interactions within and between climate-system components, rendering them irreducible. Neglecting the uncertainty induced by the ICV inevitably results in underestimation of future SLR and the associated flooding risks. Along with the spread in the sea-level changes derived from CESM1-LE, we used a realistic statistical model of large deviations in sea-level fluctuations based on previous analyses of the observed sea-level records<sup>1,34–37</sup>. The power-law model provides a simple and efficient framework for estimating ICV uncertainty in sea-level projections. The power-law statistics seem to indicate a wider range of probable sea-level changes generated by the ICV than the spread among CESM1-LE

0 members. This effect is pronounced by 2100 and under RCP 8.5 along the coasts of East Africa, west  
1 Australia, insular Southeast Asia and west United States. If the ICV uncertainty upper limit is reached, some  
2 SLR hotspots would be created in Southeast Asian megacities, making a part of at least ~20% in the expected  
3 SLR at Chennai, Kolkata, Yangon, Bangkok, Ho Chi Minh City and Manila and reaching ~30% in the  
4 western tropical Pacific Islands and in Western Indian Ocean. Considering the ICV impacts, significant  
5 changes in frequency of episodic floodings by the end of the century are expected in low-lying areas (<10 m  
6 above sea level) and densely populated regions, such as the Irrawaddy delta (Yangon), the Mekong delta  
7 (Ho Chi Minh City), several megacities (for example, Manila and Mombasa) and on the low-lying islands  
8 in the tropical Pacific, placing millions of people at risk. It is worth noting that the upper limit of  
9 steric SLR evaluated in this study should not be considered as definitive because we used a single  
0 model, and actual sea-level changes, or sea-level changes from other models, could be of somewhat different  
1 magnitude from the results presented; the spatial pattern could also differ to some degree. Note, as well, that  
2 the ICV can also attenuate regional sea level by 2100, thus masking the external trend due to global warming.  
3 In this scenario, if the ICV should swing back to increasing regional sea level by 2150 or 2200, the regional  
4 SLR will be amplified in surprising and unexpected ways. Moreover, other sources of uncertainties such as  
5 the structural model parameterization and greenhouse gas emission scenarios should be considered together  
6 with the processes not yet included in the climate models such as contributions of freshwater from ice-sheet  
7 melting and their response to ongoing climate changes.

## 9 **References**

- 0 1. Becker, M., Karpytchev, M. & Lennartz-Sassinek, S. Long-term sea level trends: natural or  
1 anthropogenic? *Geophys. Res. Lett.* **41**, 5571–5580 (2014).
- 2 2. Dangendorf, S. et al. Detecting anthropogenic footprints in sea level rise. *Nat. Commun.* **6**, 7849 (2015).
- 3 3. Kopp, R. E. et al. Temperature-driven global sea-level variability in the Common Era. *Proc. Natl Acad.*  
4 *Sci. USA* **113**, E1434–E1441 (2016).
- 5 4. Marcos, M. & Amores, A. Quantifying anthropogenic and natural contributions to thermosteric sea level  
6 rise. *Geophys. Res. Lett.* **41**, 2502–2507 (2014).
- 7 5. Meyssignac, B. et al. Tropical Pacific spatial trend patterns in observed sea level: internal variability  
8 and/or anthropogenic signature? *Climate* **8**, 787–802 (2012).
- 9 6. Slangen, A. et al. Anthropogenic forcing dominates global mean sea-level rise since 1970. *Nat. Clim.*  
0 *Change* **6**, 701–705 (2016).
- 1 7. Hasselmann, K. Stochastic climate models Part I. Theory. *Tellus* **28**, 473–485 (1976).

- 2 8. Deser, C., Phillips, A., Bourdette, V. & Teng, H. Uncertainty in climate change projections: the role of  
3 internal variability. *Clim. Dyn.* **38**, 527–546 (2012).
- 4 9. Ghil, M. in *Encyclopedia of Global Environmental Change* Vol. 1 (eds MacCracken, M. & Perry, J.)  
5 544–549 (Wiley, 2002).
- 6 10. Deser, C. Certain uncertainty: the role of internal climate variability in projections of regional climate  
7 change and risk management. *Earths Future* **8**, e2020EF001854 (2020).
- 8 11. Bordbar, M. H., Martin, T., Latif, M. & Park, W. Effects of long-term variability on projections of  
9 twenty-first century dynamic sea level. *Nat. Clim. Change* **5**, 343–347 (2015).
- 0 12. Hu, A. & Bates, S. C. Internal climate variability and projected future regional steric and dynamic sea  
1 level rise. *Nat. Commun.* **9**, 1068 (2018).
- 2 13. Hu, A. & Deser, C. Uncertainty in future regional sea level rise due to internal climate variability.  
3 *Geophys. Res. Lett.* **40**, 2768–2772 (2013).
- 4 14. Little, C. M., Horton, R. M., Kopp, R. E., Oppenheimer, M. & Yip, S.  
5 Uncertainty in twenty-first-century CMIP5 sea level projections. *J. Clim.* **28**, 838–852 (2015).
- 6 15. Meehl, G. A. et al. Initialized Earth system prediction from subseasonal to decadal timescales. *Nat. Rev.*  
7 *Earth Environ.* **2**, 340–357 (2021).
- 8 16. Sérazin, G. et al. Quantifying uncertainties on regional sea level change induced by multidecadal intrinsic  
9 oceanic variability. *Geophys. Res. Lett.* **43**, 8151–8159 (2016).
- 0 17. Slangen et al. Projecting twenty-first century regional sea-level changes. *Climatic Change* **124**, 317–332  
1 (2014).
- 2 18. Fasullo, J. T. & Nerem, R. S. Interannual variability in global mean sea level estimated from the CESM  
3 Large and Last Millennium Ensembles. *Water* **8**, 491 (2016).
- 4 19. Hu, A., Meehl, G., Stammer, D., Han, W. & Strand, W. Role of perturbing ocean initial condition in  
5 simulated regional sea level change. *Water* **9**, 401 (2017).
- 6 20. Deser, C. et al. Insights from Earth system model initial-condition large ensembles and future prospects.  
7 *Nat. Clim. Change* **10**, 277–286 (2020).
- 8 21. Kay, J. E. et al. The Community Earth System Model (CESM) Large Ensemble project: a community  
9 resource for studying climate change in the presence of internal climate variability. *Bull. Am. Meteorol.*  
0 *Soc.* **96**, 1333–1349 (2015).
- 1 22. Lyu, K., Zhang, X., Church, J. A., Slangen, A. B. A. & Hu, J. Time of emergence for regional sea-level  
2 change. *Nat. Clim. Change* **4**, 1006–1010 (2014).
- 3 23. Yip, S., Ferro, C. A., Stephenson, D. B. & Hawkins, E. A simple, coherent framework for partitioning  
4 uncertainty in climate predictions. *J. Clim.* **24**, 4634–4643 (2011).

- 5 24. Carson, M., Köhl, A. & Stammer, D. The impact of regional multidecadal and century-scale internal  
6 climate variability on sea level trends in CMIP5 models. *J. Clim.* **28**, 853–861 (2015).
- 7 25. Lyu, K., Zhang, X., Church, J. A. & Hu, J. Quantifying internally generated and externally forced climate  
8 signals at regional scales in CMIP5 models. *Geophys. Res. Lett.* **42**, 9394–9403 (2015).
- 9 26. Meyssignac, B. et al. Evaluating model simulations of twentieth-century sea-level rise. Part II: regional  
0 sea-level changes. *J. Clim.* **30**, 8565–8593 (2017).
- 1 27. Knutti, R., Furrer, R., Tebaldi, C., Cermak, J. & Meehl, G. A. Challenges in combining projections from  
2 multiple climate models. *J. Clim.* **23**, 2739–2758 (2010).
- 3 28. Murphy, J. M. et al. Quantification of modelling uncertainties in a large ensemble of climate change  
4 simulations. *Nature* **430**, 768–772 (2004).
- 5 29. Stainforth, D. A. et al. Uncertainty in predictions of the climate response to rising levels of greenhouse  
6 gases. *Nature* **433**, 403–406 (2005).
- 7 30. Harrison, C. G. A. Power spectrum of sea level change over fifteen decades of frequency. *Geochem.*  
8 *Geophys. Geosyst.* <https://doi.org/10.1029/2002GC000300> (2002).
- 9 31. Mandelbrot, B. B. & Wallis, J. R. Noah, Joseph, and operational hydrology. *Water Resour. Res.* **4**, 909–  
0 918 (1968).
- 1 32. Agnew, D. C. The time-domain behavior of power-law noises. *Geophys. Res. Lett.* **19**, 333–336 (1992).
- 2 33. Monetti, R. A., Havlin, S. & Bunde, A. Long-term persistence in the sea surface temperature  
3 fluctuations. *Physica A* **320**, 581–589 (2003).
- 4 34. Barbosa, S.M., Silva, M.E. & Fernandes, M.J. Time Series  
5 Analysis of Sea-Level Records: Characterising Long-Term  
6 Variability. In *Nonlinear Time Series Analysis in the Geosciences. Lecture Notes in Earth Sciences Vol*  
7 *112* (eds Donner, R.V. & Barbosa, S.M.) 157–173 (Springer, 2008).
- 8 35. Bos, M. S., Williams, S. D. P., Araújo, I. B. & Bastos, L. The effect of temporal correlated noise on the  
9 sea level rate and acceleration uncertainty. *Geophys. J. Int.* **196**, 1423–1430 (2013).
- 0 36. Dangendorf, S. et al. Evidence for long-term memory in sea level. *Geophys. Res. Lett.* **41**, 5530–5537  
1 (2014).
- 2 37. Marcos, M. et al. in *Integrative Study of the Mean Sea Level and Its Components Vol. 58* (eds Cazenave,  
3 A. et al.) 337–356 (Springer, 2017).
- 4 38. Becker, M., Karpytchev, M., Marcos, M., Jevrejeva, S. & Lennartz-Sassinek, S. Do climate models  
5 reproduce complexity of observed sea level changes? *Geophys. Res. Lett.* **43**, 5176–5184 (2016).
- 6 39. Peng, C.-K., Havlin, S., Stanley, H. E. & Goldberger, A. L. Quantification of scaling exponents and  
7 crossover phenomena in nonstationary heartbeat time series. *Chaos* **5**, 82–87 (1995).

- 8 40. Feder, J. *Fractals* (Springer, 1988); [https://doi.org/10.1007/978-1-](https://doi.org/10.1007/978-1-4899-2124-6)  
9 [4899-2124-6](https://doi.org/10.1007/978-1-4899-2124-6)
- 0 41. Talkner, P. & Weber, R. O. Power spectrum and detrended fluctuation analysis: application to daily  
1 temperatures. *Phys. Rev. E* **62**, 150 (2000).
- 2 42. Kantelhardt, J. W., Koscielny-Bunde, E., Rego, H. H., Havlin, S. & Bunde, A. Detecting long-range  
3 correlations with detrended fluctuation analysis. *Physica A* **295**, 441–454 (2001).
- 4 43. Gregory, J. M. et al. Concepts and terminology for sea level: mean, variability and change, both local  
5 and global. *Surv. Geophys.* **40**, 1251–1289 (2019).
- 6 44. Monselesan, D. P., O’Kane, T. J., Risbey, J. S. & Church, J. Internal climate memory in observations  
7 and models. *Geophys. Res. Lett.* **42**, 1232–1242 (2015).
- 8 45. Bloomfield, P. & Nychka, D. Climate spectra and detecting climate change. *Climatic Change* **21**, 275–  
9 287 (1992).
- 0 46. Lennartz, S. & Bunde, A. On the estimation of natural and anthropogenic trends in climate records. In  
1 *Extreme Events and Natural Hazards: The Complexity Perspective* (eds A.S. Sharma,  
2 A. Bunde, V.P. Dimri & D.N. Baker) 177–189 (2012). [https://doi.org/](https://doi.org/10.1029/2011GM001079)  
3 [10.1029/2011GM001079](https://doi.org/10.1029/2011GM001079)
- 4 47. Gulev, S. K. et al. Changing state of the climate system. In *Climate Change 2021: The Physical Science*  
5 *Basis*. Contribution of Working Group I to the Sixth Assessment Report of the Intergovernmental Panel  
6 on Climate Change 287–422 (2021).
- 7 48. Lennartz, S. & Bunde, A. Trend evaluation in records with long-term memory: application to global  
8 warming. *Geophys. Res. Lett.* **36**, L16706 (2009).
- 9 49. Tamazian, A., Ludescher, J. & Bunde, A. Significance of trends in long-term correlated records. *Phys.*  
0 *Rev. E* **91**, 032806 (2015).
- 1 50. Deser, C., Phillips, A. S., Alexander, M. A. & Smoliak, B. V. Projecting North American climate over  
2 the next 50 years: uncertainty due to internal variability. *J. Clim.* **27**, 2271–2296 (2014).
- 3 51. Hinkel, J. et al. Sea-level rise scenarios and coastal risk management. *Nat. Clim. Change* **5**, 188–190  
4 (2015).
- 5 52. Pugh, D. T. *Tides, Surges and Mean Sea-Level: A Handbook for Engineers and Scientists* (Wiley, 1987).
- 6 53. Hunter, J. Estimating sea-level extremes under conditions of uncertain sea-level rise. *Climatic Change*  
7 **99**, 331–350 (2010).
- 8 54. Hunter, J. R., Woodworth, P. L., Wahl, T. & Nicholls, R. J. Using global tide gauge data to validate and  
9 improve the representation of extreme sea levels in flood impact studies. *Glob. Planet. Change* **156**, 34–  
0 45 (2017).

- 1 55. Hunter, J. A simple technique for estimating an allowance for uncertain sea-level rise. *Climatic Change*  
2 **113**, 239–252 (2012).
- 3 56. Slangen et al. The impact of uncertainties in ice sheet dynamics on sea-level allowances at tide gauge  
4 locations. *J. Mar. Sci. Eng.* **5**, 21 (2017).
- 5 57. Woodworth, P. L., Hunter, J. R., Marcos, M. & Hughes, C. W.  
6 Towards reliable global allowances for sea level rise. *Glob. Planet. Change* **203**, 103522 (2021).
- 7 58. Almar, R. et al. A global analysis of extreme coastal water levels with implications for potential coastal  
8 overtopping. *Nat. Commun.* **12**, 3775 (2021).
- 9 59. Hoornweg, D. & Pope, K. Population predictions for the world’s largest cities in the 21st century.  
0 *Environ. Urban.* **29**, 195–216 (2017).

## 1 **Methods**

### 2 **Model and experiments**

3 **Model.** The CESM1 is a global-scale and fully coupled climate model developed at the National Center for  
4 Atmospheric Research and by the US Department of Energy laboratories<sup>60</sup>. The model is performed with 1°  
5 latitude/longitude resolution for all components and with an enhanced resolution for the ocean component  
6 in the equatorial regions. The CESM1 runs used in this study do not include an active ice-sheet model,  
7 glacial isostatic adjustment and gravitational force changes. As such, it allows us to estimate only the steric  
8 and dynamic sea-level changes, which together account for ~40% of the observed global mean SLR for  
9 recent decades. The net heat gain and loss by the ocean, generating the sea-level fluctuations, is computed  
0 as the vertical integration of the seawater in situ density and summed globally. The thermosteric sea-level  
1 variations added to the dynamic sea-level field obtained from the model simulations provide the regional  
2 SLR.

3 **Experiments.** The LE simulations used in this study start from the same twentieth-century all-forcing  
4 simulation branched from the 1850 pre-industrial CESM1 control simulation (Extended Data Fig. 1). A  
5 round-off level perturbation is introduced into the air temperature field on 1 January 1920 from the ensemble  
6 member number 1 (ens001; Extended Data Fig. 1) and is run to 2005 (40 members in total). After 2005, the  
7 simulations follow RCP 8.5 from 2006 to 2100. For details of the experimental design, please see (ref. <sup>2</sup>).  
8 The CESM1-LE includes also a 1,800 yr fully coupled pre-industrial control run in which all external forcing  
9 is set to constant at pre-industrial level (1850); for example, CO<sub>2</sub> concentration is 284 parts per million by  
0 volume.

1 All the datasets are freely available on the CESM webpage: [http://](http://www.cesm.ucar.edu/projects/community-projects/LENS/data-sets.html)  
2 [www.cesm.ucar.edu/projects/community-projects/LENS/data-sets.html](http://www.cesm.ucar.edu/projects/community-projects/LENS/data-sets.html).

### 3 **DFA and the scaling exponent ( $\alpha$ )**

4 The DFA $n$  is designed to study long-term correlations in time series in the presence of external trends<sup>42</sup>. The  
5 DFA $n$  filters out local polynomial trends up to the  $n$  order when constructing a fluctuation function  $F(s) \sim s^\alpha$ ,  
6 with  $s$  the time-window size and  $\alpha$  the scaling exponent. Depending on the value of the scaling exponent  $\alpha$ ,  
7 different signal characteristics can be identified as uncorrelated signal for  $\alpha = 0.5$  (white noise) and long-  
8 term correlations for  $\alpha > 0.5$  (see (ref. <sup>42</sup>) for more details about the DFA).

9 Here we briefly present the main steps of the DFA $n$  procedure for a record  $X(i)$ ,  $i = 1 \dots L$ :

- 0 • Compute the integration profile  $Y(i) = \sum_{k=1}^i [X_k - \bar{X}]$ ,  $i = 1 \dots L$  where  
1  $\bar{X} = \frac{1}{L} \sum_{i=1}^L X_i$
- 2 • Determine the number of intervals of equal length  $i=1 \dots L$   $s: L_s L ] = \lfloor s$
- 3 • Divide  $Y(i)$  into  $L_s$  non-overlapped intervals of equal length  $s$
- 4 • Fit on  $Y(i)$  for each interval  $v = 1, \dots, L_s$  a polynomial of order  $n$ , called  $p_v^n(i)$
- 5 • Subtract the polynomial for each interval  $v$  and estimate the variance:  $F_v^2(s) = \frac{1}{s} \sum_{i=1}^{L_s} [Y_v((v-1)s + i) - p_v^n(i)]^2$
- 6 • Repeat this procedure for all timescales  $s$
- 7 • Establish the ‘fluctuation function’  $F^{(s)} = \sqrt{\frac{1}{L_s} \sum_{v=1}^{L_s} F_v^2(s)}$
- 8 • Determine the scaling exponent  $\alpha$  given by the slope of the regression line between  $\log(s)$  and  $\log(F(s))$ .

9 In this study, following (refs. <sup>42,49</sup>), the scaling exponent  $\alpha$  of stereodynamic sea-level fluctuations is  
0 estimated on each grid point of the 1,800 yr monthly CESM1 pre-industrial control run<sup>21</sup> by DFA3 with  
1 windows of size  $s$  ranging from 1 to 95 yr. By definition, DFA3 removes cubic trends in the profile  $Y(i)$  and  
2 thus quadratic trends in the original series  $X(i)$ . To limit a bias in the scaling exponent  $\alpha$  estimation due to  
3 oscillations<sup>42</sup>, at each CESM1 grid point, the sea-level seasonal signal was removed before analysis by  
4 subtracting the mean for each month. The inverted barometric correction is not applied as this correction has  
5 no significant effect on the scaling exponent estimation<sup>36</sup>.

### 6 **Expected sea-level change and ICV uncertainty from CESM1-LE**

7 To evaluate the long-term changes in the mean of sea-level variations at the end of the considered period we  
8 (1) evaluate the slope of the linear trend (cm yr<sup>-1</sup>) of a sea-level time series over 1920–2005 and (2) multiply  
9 this slope by the duration of the sea-level time series, 86 yr (for example, with a slope = 0.3 cm yr<sup>-1</sup>, sea-  
0 level increase in 2005 relative to 1920 is  $0.3 \times 86 = 26$  cm). The resulting value,  $\Delta_{\text{histo}_{i=1 \dots 40}}$ , is called the  
1 expected sea-level change (Extended Data Fig. 2). However, we also evaluate the expected mean sea-level  
2 change due to external forcing as the mean  $\Delta_{\text{histo}_{i=1 \dots 40}}$ , and  $2\sigma$  of the set of  $\Delta_{\text{histo}_{i=1 \dots 40}}$  measures the ICV

3 contribution to the mean sea-level changes by 2005 relative to 1920 (called  $ICV_{CESM1-LE}$ ; Fig. 2).  
4 Considering the 40-member CESM1-LE RCP 8.5 over 2006–2100, in the same way, we define  
5  $\Delta RCP8_{i=1\dots405}$  as the expected forced sea-level changes,  $\Delta RCP8_{i=1\dots405}$  as the expected forced mean sea-  
6 level changes (Fig. 3b) and  $2\sigma$  of the set of  $\Delta RCP8_{i=1\dots405}$  as the ICV contribution to the mean sea-level  
7 changes by 2100 relative to 2006 (Extended Data Fig. 4).

### 9 **Expected sea-level change and ICV uncertainty from power-law statistics**

0 Several studies<sup>46,48,49</sup> have established the probability that a regression line drawn through a Gaussian long-  
1 term correlated times series rises up spontaneously to some level  $\Delta$ , corresponding to the difference between  
2 the first and last points of the linear regression line, which are not necessarily the first and the last points of  
3 the time series considered (Extended Data Fig. 3). The non-dimensional increase  $x$  is introduced by a ratio  
4  $x = \Delta/\sigma_t$ , with  $\sigma_t$  the standard deviation of the dispersion around the linear regression line (Extended Data Fig.  
5 3). Note that  $\sigma_t$  is not perturbed by the presence of external trend and represents the natural fluctuations.  
6 (Ref. 48) determined the probability  $P(x, \alpha, L)dx$  that in a long-term correlated time series of length  $L$ ,  
7 characterized by a scaling exponent  $\alpha$ , a spontaneous trend occurs with a slope between  $x$  and  $x + dx$ . The  
8 exceedance probability  $W(x, \alpha, L) = \int_x^\infty P(x', \alpha, L)dx'$  gives a probability that the spontaneous trend has a slope larger  
9 than  $x$ . The confidence bounds are then obtained from the exceedance probability  $W(x, \alpha, L)$ :  $x_Q = W^{-1}((1$   
0  $- Q)/2, \alpha, L)$ . Hence, to a confidence level of 95% ( $Q = 0.95$ ), we estimate the upper and lower limits ( $\pm x_{95}$ )  
1 of the part of the observed trend that can be fully explained by the natural variability, that is, due to the ICV  
2 uncertainty (see (refs. 46,48,49) for more details). Finally, by multiplying  $\pm x_{95}$  by the standard deviation,  $\sigma_t$ ,  
3 we estimate the probable ICV contribution to the observed trend, called  $ICV_{power-law}$  (Fig. 2). In this study,  
4 for each CESM1 grid point, the scaling exponent  $\alpha$  is obtained from the monthly 1,800 yr CESM1 pre-  
5 industrial control run;  $L = 86$  yr (1,032 months), corresponding to the length of the CESM1-LE historical  
6 simulations period 1920–2005 (CESM1-LE RCP 8.5: 95 yr to 2006–2100);  $\Delta$  and  $\sigma_t$  are estimated from one  
7 member of CESM1-LE historical simulations over 1920–2005 (over 2006–2100 for CESM1-LE RCP 8.5);  
8 and the confidence level is fixed at  $Q = 0.95$ . Hence, the upper limits of  $ICV_{power-law}$  are considered as the  
9 maximum expected ICV contribution to sea-level change, by 2100 relative to 2006, obtained from the  
0 power-law statistics (Fig. 3a).

### 2 **Data availability**

3 All the CESM1-LE datasets are freely available on the Community Earth System Model webpage:  
4 [http://www.cesm.ucar.edu/projects/ community-projects/LENS/data-sets.html](http://www.cesm.ucar.edu/projects/community-projects/LENS/data-sets.html). The World Port Index

5 database is provided by the National Geospatial-Intelligence Agency and is freely available at  
6 <https://msi.nga.mil/Publications/WPI>.

## 7 **References**

8 60. Hurrell, J. W. et al. The Community Earth System Model: a framework for collaborative research. *Bull.*  
9 *Am. Meteorol. Soc.* **94**, 1339–1360 (2013).

## 0 **Acknowledgements**

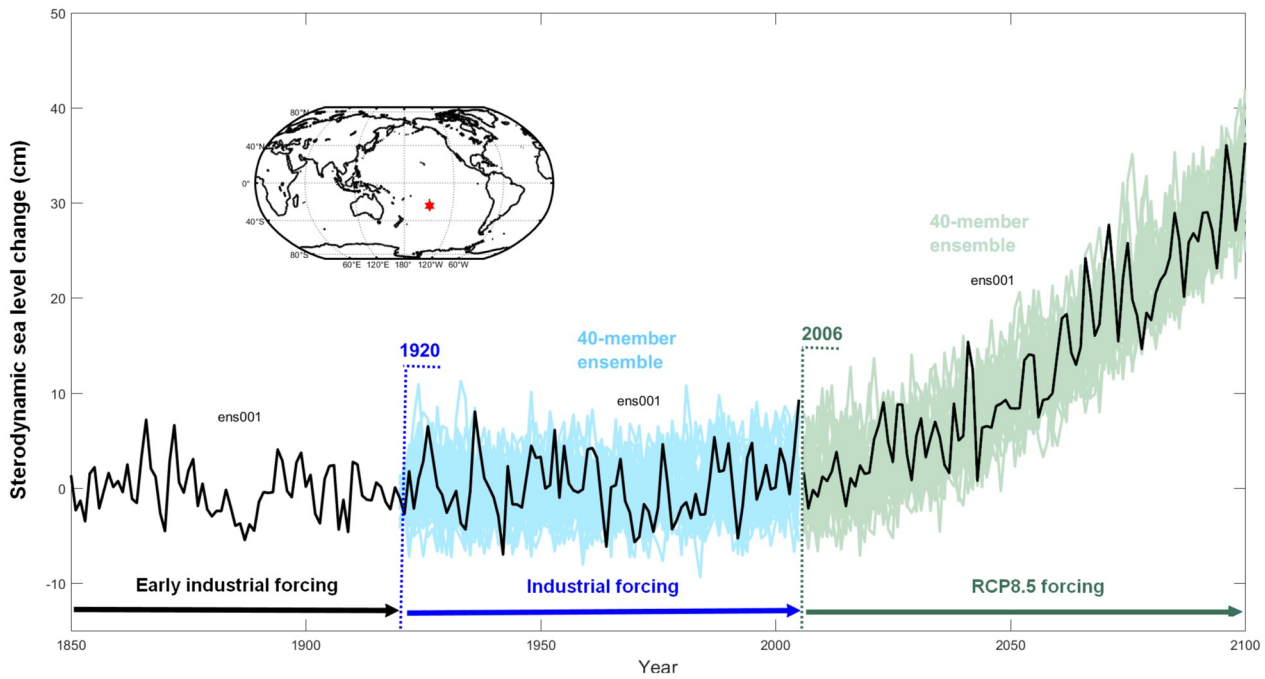
1 This work was supported by the French Research Agency (Agence Nationale de la Recherche [ANR]) under  
2 the Deltas Under Global Impact of Change (DELTA) project (ANR-17-CE03-0001) and by the Centre  
3 National d'Etudes Spatiales (CNES) through the project Terre Solide, Océan, Surfaces Continentales et  
4 Atmosphère (TOSCA)/ GEOMINING. A.H. was supported by the Regional and Global Model Analysis  
5 (RGMA) component of the Earth and Environmental System Modeling Program of the US Department of  
6 Energy's Office of Biological and Environmental Research (BER) via National Science Foundation IA  
7 1844590. This research used resources of the National Energy Research Scientific Computing Center, a  
8 DOE Office of Science User Facility supported by the Office of Science of the US Department of Energy  
9 under contract no. DE-AC02-05CH11231 and resources from the Climate Simulation Laboratory at NCAR's  
0 Computational and Information Systems Laboratory, sponsored by the National Science Foundation and  
1 other agencies. We are grateful to C. Deser for helpful and encouraging discussions.

## 2 **Author contributions**

3 M.B., M.K. and A.H. conceived the study. M.B. performed the analysis and conducted the computations.  
4 M.B., M.K. and A.H. discussed the results and wrote the manuscript.

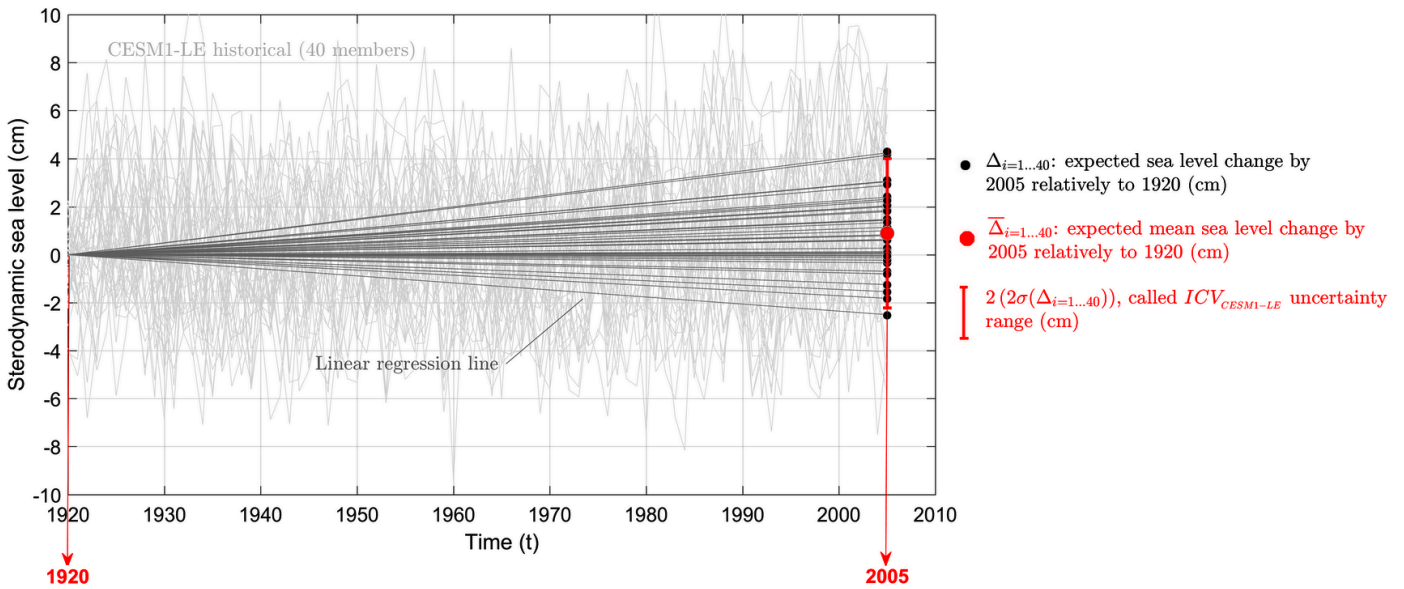
5

6



7 **Extended Data Fig. 1 | CESM1 Large Ensemble.** The CESM1 Large Ensemble data sets.

8

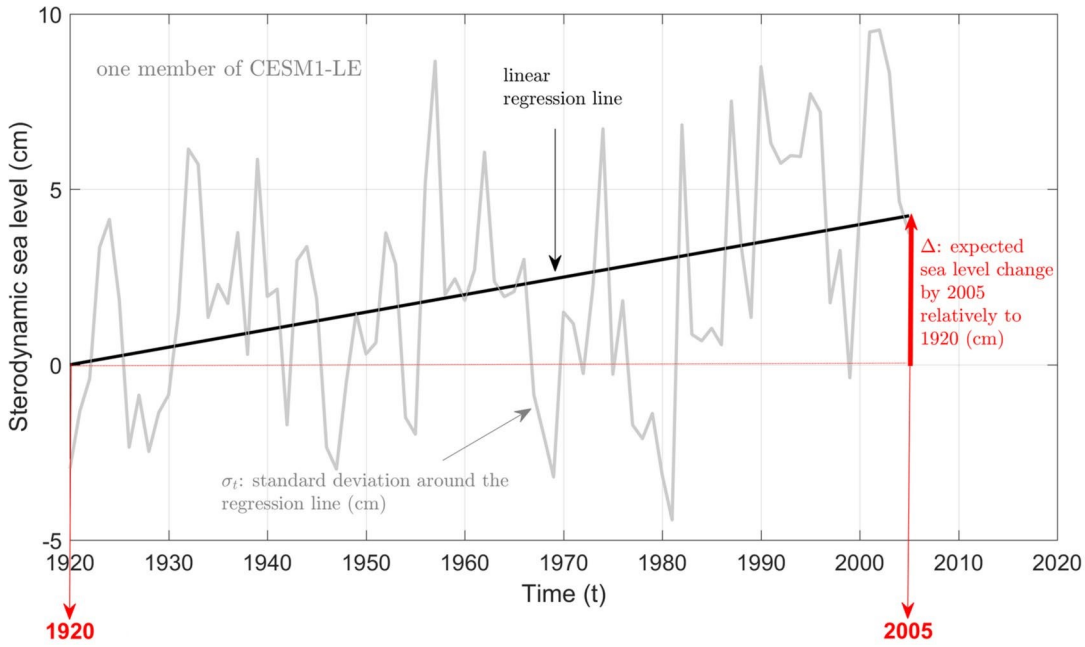


9

0

1 **Extended Data Fig. 2 | The sea level changes simulated by CESM1-LE.** The 40 gray lines are the sea  
 2 level changes simulated at one grid point by the 40-members of the CESM1-LE historical simulations over  
 3 1920-2005. The expected sea level change is measured by  $\Delta$ ,  $\bar{\Delta}$  and  $ICV_{CESM1-LE}$  which are computed as  
 4 described in the text.

5



6

7

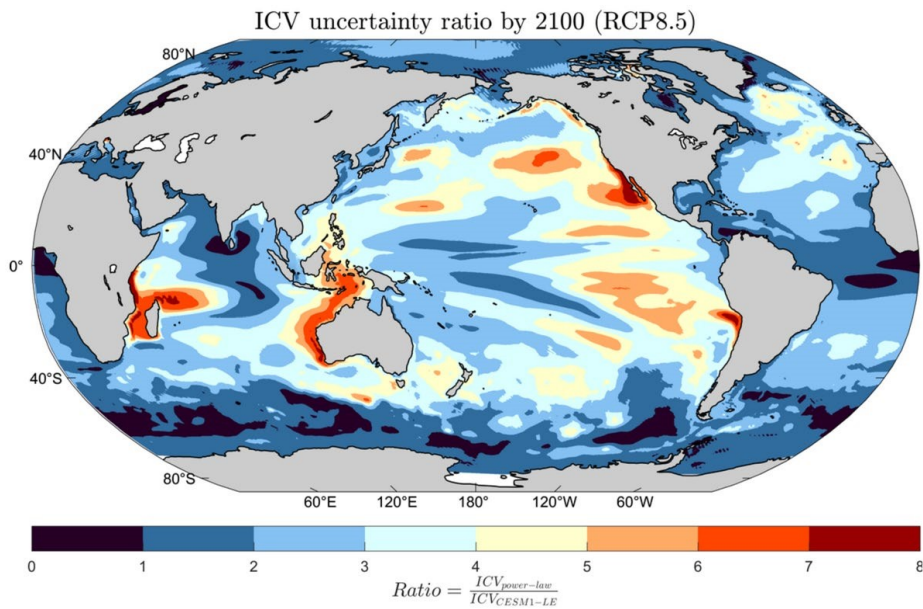
**Extended Data Fig. 3 | Visualization of the considered quantities  $\Delta$  and  $\sigma_t$ .** These quantities are obtained from one member of CESM1-LE historical simulation, at a given grid point, over 1920–2005.

8

9

0

1



2

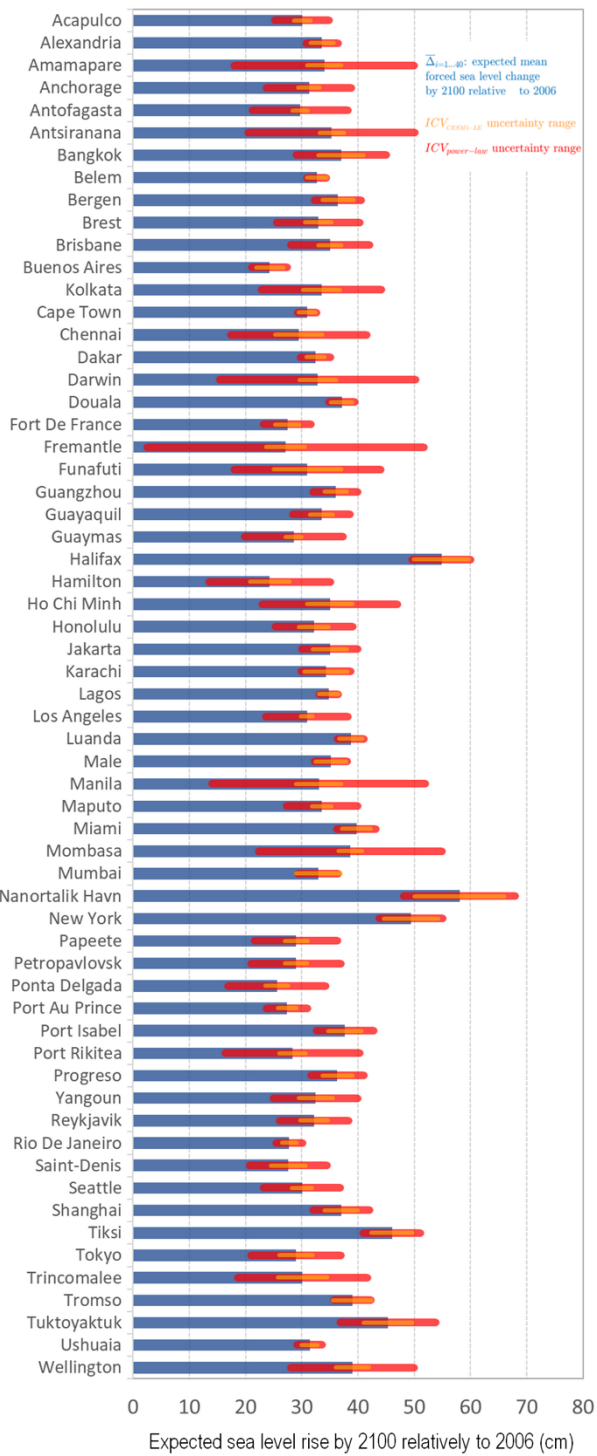
**Extended Data Fig. 4 | Comparison of the ICV contributions.** Ratio of ICV contribution to the expected sea level changes between  $ICV_{power-law}$  obtained from the power-law statistics (two-sided 95% confidence level) and  $ICV_{CESM1-LE}$  provided by the spread ( $2\sigma$ ) between the  $\Delta_i=1\dots 40$  from the 40-members CESM1-LE under RCP8.5 by 2100 relative 2006.

3

4

5

6  
7  
8  
9  
0  
1  
2  
3  
4  
5  
6  
7  
8  
9  
0  
1  
2  
3  
4  
5  
6  
7  
8  
9  
0  
1  
2  
3  
4  
5  
6  
7  
8  
9  
0  
1  
2



**Extended Data Fig. 5 | Expected externally forced sea level rise by 2100 of** obtained from the power-law statistics. In orange: ICV<sub>CESM1-LE</sub> from the spread **major ports world-wide**. Expected externally forced sea level rise (cm, in blue) ( $2\sigma$ ) between 40-members CESM1-LE. The sites are major ports world-wide (the by 2100 relative to 2006 under a carbon high-emissions global warming scenario World

7 Port index database <https://msi.nga.mil/Publications/WP>) (that is RCP8.5). In red:  $ICV_{power-law}$  range (two-  
8 sided 95% confidence level)